Langerin negative dendritic cells promote potent CD8$^+$ T-cell priming by skin delivery of live adenovirus vaccine microneedle arrays

Veronique Bachy[a,1], Catherine Hervouet[a,1], Pablo D. Becker[a], Laurent Chorro[b], Leo M. Carlin[b], Shanthi Herath[a], Timos Papagatsias[c], Jean-Baptiste Barbaroux[d], Sea-Jin Oh[e], Adel Benlahrech[c], Takis Athanasopoulos[f], George Dickson[f], Steven Patterson[c], Sung-Yun Kwon[e], Frederic Geissmann[b], and Linda S. Klavinskis[a,2]

[a]Peter Gorer Department of Immunobiology, [b]The Centre for Molecular and Cellular Biology of Inflammation, and [d]St John's Institute of Dermatology, King's College School of Medicine, London SE1 9RT, United Kingdom; [c]Department of Immunology, Imperial College London, London SW10 9NH, United Kingdom; [e]TheraJect, Inc., Fremont, CA 94538; and [f]School of Biological Sciences, Royal Holloway-University of London, Egham TW20 0EX, United Kingdom

Edited by Rafi Ahmed, Emory University, Atlanta, GA, and approved January 15, 2013 (received for review August 31, 2012)

Stabilization of virus protein structure and nucleic acid integrity is challenging yet essential to preserve the transcriptional competence of live recombinant viral vaccine vectors in the absence of a cold chain. When coupled with needle-free skin delivery, such a platform would address an unmet need in global vaccine coverage against HIV and other global pathogens. Herein, we show that a simple dissolvable microneedle array (MA) delivery system preserves the immunogenicity of vaccines encoded by live recombinant human adenovirus type 5 (rAdHu5). Specifically, dried rAdHu5 MA immunization induced CD8$^+$ T-cell expansion and multifunctional cytokine responses equipotent with conventional injectable routes of immunization. Intravital imaging demonstrated MA cargo distributed both in the epidermis and dermis, with acquisition by CD11c$^+$ dendritic cells (DCs) in the dermis. The MA immunizing properties were attributable to CD11c$^+$ MHCII^{hi} CD8α^{neg} epithelial cell adhesion molecule (EpCAM^{neg}) CD11b$^+$ langerin (Lang; CD207)^{neg} DCs, but neither Langerhans cells nor Lang$^+$ DCs were required for CD8$^+$ T-cell priming. This study demonstrates an important technical advance for viral vaccine vectors progressing to the clinic and provides insights into the mechanism of CD8$^+$ T-cell priming by live rAdHu5 MAs.

Infection with HIV, malaria, and tuberculosis represents a global public health challenge. Candidate vaccines based on live recombinant viral vectors such as adenovirus (Ad), CMV, and poxvirus show promise through their ability to induce strong T-cell immunity (1–3). However, live vaccines are thermolabile, with loss in potency and safety in the absence of continuous cold chain storage and transport. Lyophilization has been used to stabilize virus/vector infectivity (4, 5), yet, in resource limited settings, this approach is constrained by the need for sterile reconstitution, safe injection, and trained staff. This situation creates risks of blood borne disease transmitted from contaminated needles and syringes and, once reconstituted, lyophilized vaccines rapidly loose potency, incurring wastage and increased cost (5), highlighting a critical unmet need, for vaccines that enable ease of administration with long-term viral vector thermostability. Therefore, it would be invaluable to combine the heat stability of a dry vaccine with technology that introduced "live" vaccine antigens (Ags) by needle-free administration that had the capacity to harness the Ag presenting capacity of tissue resident dendritic cells (DCs) in the skin.

Developments in microfabrication technology have enabled ultrasharp, micrometer-scale projections to penetrate the skin, containing lyophilized vaccine coated on metallic structures or encapsulated within dissolvable polymers (6–8). Designs under evaluation have largely been restricted to nonlive vaccine platforms (6, 8–10). However, for HIV, induction of high frequency protective CD8$^+$ T-cell responses will require high levels of Ag expression in the context of a potent inflammatory response that has been achieved by live recombinant Ad vectors in preclinical models (1). However, the capacity of this new generation of live recombinant vaccines to prime CD8$^+$ T cells as dried microneedle arrays (MAs) via the skin has largely been unexplored. Although intense interest has focused on the physical parameters of microneedle fabrication (7, 11), little attention has been paid to the type of skin DCs subsets mobilized by this vaccine platform. The potential for different DCs subsets—epidermal Langerhans cells (LCs), dermal Langerin (Lang, also called CD207) positive, and Lang^{neg} DCs (12)—to promote distinct and opposing Ag-specific responses (13) offers opportunities to further optimize vaccine responses by targeting specific DC subtypes.

Here, we describe a dissolvable MA delivery system with the capacity to preserve the bioactivity of live rAdHu5 vectors and induce potent multifunctional CD8$^+$ T-cell responses in mice both to a model Ag ovalbumin (OVA) and a candidate HIV-1 group specific antigen (gag) vaccine. Furthermore, we demonstrate a critical role for CD11c$^+$ MHCII^{hi} CD8α$^-$ epithelial cell adhesion molecule (EpCAM)^{neg} CD11b$^+$ CD103$^-$ Lang$^-$ DC in priming the CD8$^+$ T-cell response, which intriguingly is driven independently of Lang$^+$ DCs, which include LCs and Lang$^+$ DCs.

Results

Dried Live rAdHu5 Vectored MA Vaccine Retains Thermostability and Induces Multifunctional CD8$^+$ T Cells via Skin Delivery. We first determined whether rAdHu5 vectors could be dried at room temperature and stored without loss of immunogenicity by using sodium carboxymethylcellulose (Na-CMC), a biocompatible, mechanically strong, highly water soluble polymer (14) suitable for microneedle fabrication and sucrose, an established protein stabilizer. A rAdHu5 vector expressing chicken ovalbumin (OVA) air dried and stored under desiccation at 25 °C up to 1 mo demonstrated no statistically significant loss in immunogenicity, determined by K^b/SIINFEKL pentamer staining as a measurement of CD8$^+$ T-cell induction to an immunodominant OVA epitope, when reconstituted and injected s.c. in B6 mice compared with the control virus stored at −80 °C that contained an equivalent virus titer and was injected in parallel (Fig. 1*A*). To evaluate the potential of the dried rAdHu5 formulation in a needle-free delivery system, dissolvable microneedles (1,500 μm in length, 44 per array) were fabricated within a silicone template. The Na-CMC-sucrose matrix containing virus and tetramethyl rhodamine (TR) dextran (for visualization) formed the needle tips (Fig. 1 *B* and *C*). Mechanical strength was added by layering a second matrix [12% (wt/vol) Na-CMC, 4.8% (wt/vol)

Author contributions: V.B., C.H., and L.S.K. designed research; V.B., C.H., P.D.B., L.C., L.M.C., S.H., and J.-B.B. performed research; T.P., S.-J.O., and S.-Y.K. contributed new reagents/analytic tools; V.B., C.H., P.D.B., L.C., L.M.C., S.H., T.P., J.-B.B., A.B., T.A., G.D., S.P., F.G., and L.S.K. analyzed data; and F.G. and L.S.K. wrote the paper.

Conflict of interest statement: S.-Y.K. and S.-J.O. are shareholders in THeraject that holds the patent rights for dissolvable microneedle arrays for vaccine delivery.

This article is a PNAS Direct Submission.

[1]V.B. and C.H. contributed equally to this work.

[2]To whom correspondence should be addressed. E-mail: linda.klavinskis@kcl.ac.uk.

This article contains supporting information online at www.pnas.org/lookup/suppl/doi:10.1073/pnas.1214449110/-/DCSupplemental.

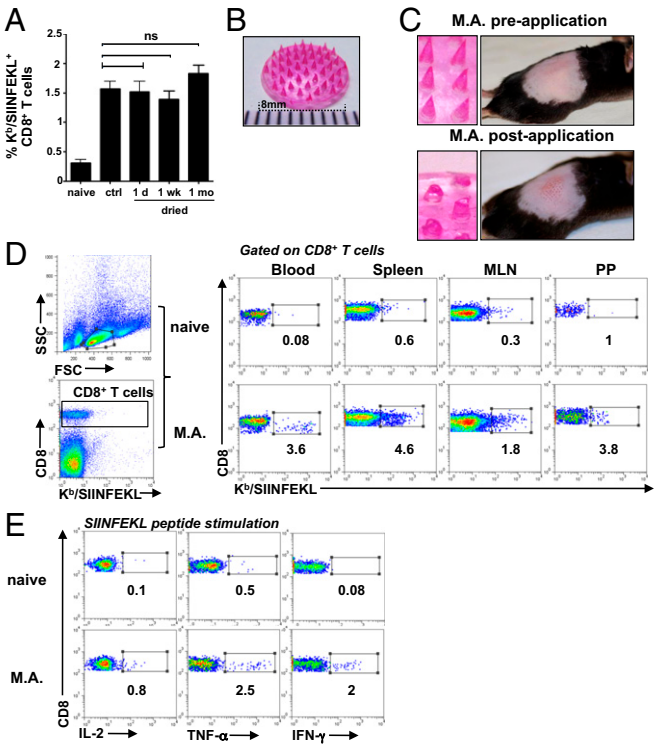

Fig. 1. Dried rAdHu5 vectored vaccines retain thermostability and induce functional CD8$^+$ T cells when fabricated into dissolvable MAs. (*A*) Frequency of SIINFEKL-specific CD8$^+$ T cells 10 d after s.c. immunization with rAdHu5-OVA (4.3×10^8 vp) either after air drying up to 1 mo in a sucrose-Na-CMC gel on plastic and redissolved in PBS or the same virus dose stored in buffer at −80 °C (control virus; ctrl) relative to naïve mice. Data indicate the mean ± SEM (of six to eight mice per group) pooled from two independent experiments. (*B*) MA fabricated with rAd5Hu-OVA and TR-dextran in a sucrose-Na-CMC matrix. (Scale bar divisions: 1 mm.) (*C*) MAs and en face view of B6 back skin before (*Upper*) and (5 min) after (*Lower*) MA application. (*D*) Dot plots of Kᵇ/SIINFEKL-specific CD8$^+$ T cells in blood, spleen, MLN, and Peyer's patches (PP) of naïve mice (*Upper*) and 14 d after immunization with rAd5Hu-OVA via M.A (*Lower*). (*E*) Frequency of SIINFEKL-specific cytokine (IL-2, TNF-α, and IFN-γ) producing CD8$^+$T cells in spleen of naïve mice (*Upper*) and 14 d after rAdHu5-OVA MA immunization (*Lower*) stimulated 6 h ex vivo with SIINFEKL peptide and assessed by flow cytometry. Values (*D* and *E*) represent percentage of cells in each gate and are representative of three naïve and eight vaccinated mice.

lactose] creating the needle shaft and applying a premade membrane [8% (wt/vol) Na-CMC, 0.8% lactose) to the needle base. Each array contained an average of 7.8×10^8 virus particles (vp) of rAdHu5 vector determined by virus recovery. The MAs dissolved within 5 min of application by gentle pressure to the skin of B6 mice and, after removal, were reduced by approximately two-thirds in length (Fig. 1*C*), depositing on average 4.3×10^8 vp of rAdHu5 vector in the skin. At day 10 after immunization, a high frequency of Kᵇ/SIINFEKL pentamer-specific CD8$^+$ T cells were tracked in the systemic compartment (blood and spleen) and also mucosal tissues [mesenteric lymph node (MLN) and Peyer's patches], exemplified in Fig. 1*D*. To assess their function, CD8$^+$ T cells from the spleen were analyzed by multiparameter flow cytometry for intracellular IL-2, TNF-α, and IFN-γ after ex vivo stimulation with $OVA_{257–264}$ (Fig. 1*E*) or IFN-γ, TNF-α, and CD107a (Fig. S1). Consistent with previous human adenovirus type 5 (AdHu5) vaccine immunization studies by conventional i.m. injection (15, 16), the MAs induced robust IFN-γ and TNF-α–producing CD8$^+$ T cells with low levels of intracellular IL-2 (Fig. 1*E*), and also high-frequency CD8$^+$ T cells with up-regulation of CD107a that also secreted IFN-γ or TNF-α (Fig. S1). These results indicate that a single immunization with a dried live rAdHu5 vectored MA retained the capacity to induce multifunctional CD8$^+$ T cells.

Dried rAdHu5 Vectored MAs Induce Primary CD8$^+$ T-Cell Responses Equipotent with Conventional Injectable Routes of Systemic Vaccine Delivery. To test the T-cell priming efficiency afforded by dried rAdHu5 MAs compared with conventional routes of immunization, we injected groups of B6 mice with the equivalent dose of rAdHu5-OVA virus in solution by either the intradermal (i.d.), s.c., or i.m. route and by dried MA application to skin. Kᵇ/SIINFEKL pentamer-specific CD8$^+$ T-cell expansion was determined in blood at day 13 and, also, in spleen, MLN, and Peyer's patches at day 14. The frequency of SIINFEKL-specific CD8$^+$ T cells induced by MA immunization when cross-compared with each other route of immunization was statistically indistinguishable (Fig. 2*A*) and was also comparable with the i.m. route at a lower vector dose (Fig. S2). Interestingly, a trend toward an increased frequency of SIINFEKL-specific CD8$^+$ T cells induced in Peyer's patches of MA primed relative to the i.m. or s.c. primed mice was observed (Fig. 2*A*). Consistent with this observation, splenocytes from MA.-primed mice expressed a significant increase in the α4β7 mucosal homing marker on SIINKFEKL-specific CD8$^+$ T cells compared with s.c. or i.m. immunized mice ($P < 0.05$; Fig. 2*B*) but was not significantly different from i.d. immunization ($P = 0.057$). Moreover, both routes induced comparable amounts of IFN-γ– and IL-2–producing $OVA_{257–264}$-specific CD8$^+$ T cells (Fig. 2*C*).

MA Delivery of a Dried rAdHu5 HIV-1 Gag Vaccine Candidate Induces Efficient IFN-γ Producing Cytolytic T-Cell Responses in Vivo. Next we tested the efficiency of T-cell priming by rAdHu5 MA immunization in the setting of a relevant vaccine target, as opposed to a highly immunogenic model Ag. To that end, a rAdHu5 vector encoding a synthetic HIV-1 strain CN54 gag gene optimized for mammalian codon use and cytoplasmic expression was generated and then delivered by dried MA and the equivalent dose by i.d. injection. CD8$^+$ T-cell frequencies induced by both routes were comparable and showed no statistical significance in blood, spleen, inguinal, and mesenteric lymph nodes (LNs) when tracked by tetramer to the immunodominant Dᵇ-restricted HIV-1 CN54 $gag_{309–318}$ epitope (Fig. 3*A*). Moreover, these CD8$^+$ T cells were long lived and were boosted up to at least 1 y after MA immunization (Fig. S3). To probe functional responsiveness of primed T cells, we restimulated splenocytes ex vivo with an MHC I-restricted HIV-1 CN54 $gag_{309–318}$ peptide. The frequency of IFN-γ producing CD8$^+$ T cells induced by the MA vaccine was robust, and compared with i.d.-injected mice (Fig. 3*B*), the differences were not significant. Ultimately, the efficiency of CD8$^+$ epitope-specific CTL

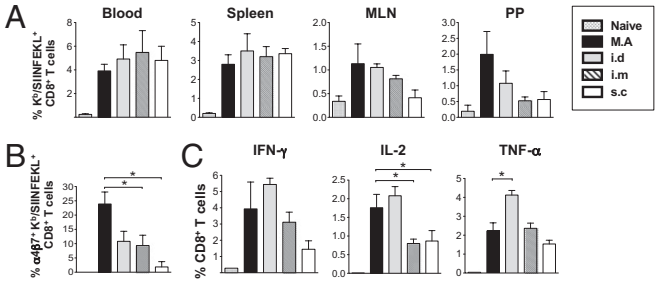

Fig. 2. Dried rAdHu5 vectored MAs induce primary CD8$^+$ T-cell responses equipotent with conventional injected routes of vaccine delivery. Mice were immunized with the same dose of rAdHu5-OVA delivered by MA, or i.d., i.m., or s.c. injection and analyzed on day 14. (*A*) Frequency of Kᵇ/SIINFEKL-specific CD8$^+$ T cells in blood, spleen, MLN, and PP. (*B*) Frequency of α4β7$^+$ Kᵇ/SIINFEKL$^+$ CD8$^+$ T cells in spleen. (*C*) IFN-γ, IL-2, and TNF-α secretion by CD8$^+$ T cells from spleen stimulated ex vivo with SIINFEKL peptide (5 μg/mL) and assessed by flow cytometry. Data are the mean ± SEM of three to six mice per group, representative of three independent experiments. *$P < 0.05$, ANOVA followed by Tukey–Kramer post hoc test.

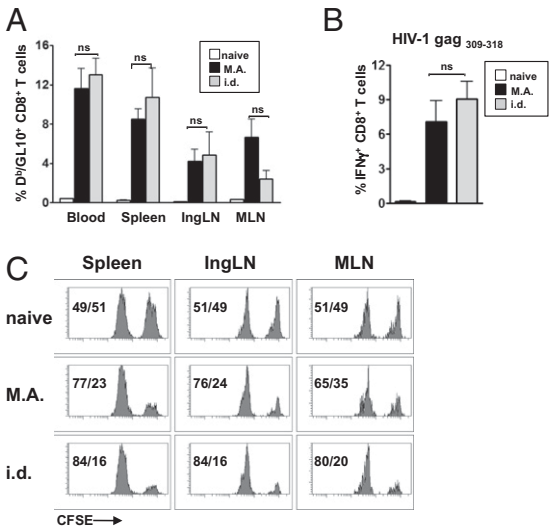

Fig. 3. Vaccination of mice with live rAdHu5 HIV-1 CN54 gag by dried MA elicits HIV gag-specific $CD8^+$ T cells of high frequency and in vivo cytolytic effector function. Mice were vaccinated with the equivalent dose of rAdHu5 HIV-1 CN54 gag by dried MA or by i.d. needle injection and analyzed on day 14. (*A*) Frequency of $CD8^+$ T cells to the immunodominant D^b-restricted HIV-1 gag CN54 (GL10) epitope detected by D^b/GL10 tetramer staining in blood, spleen, inguinal LN, and MLN. (*B*) Frequency of HIV-1 CN54 $gag_{309–318}$-specific IFN-γ–producing $CD8^+$ T cells in spleen assessed by flow cytometry after ex vivo stimulation with peptide. (*A* and *B*) Data are the mean ± SEM of $n = 3$ naïve and $n = 8$ immunized mice per group and is representative of three independent experiments. (*C*) In vivo cytolysis of CFSE-labeled splenocytes pulsed with HIV-1 CN54 $gag_{309–318}$ peptide ($CFSE^{hi}$) or no Ag ($CFSE^{lo}$) in spleen, inguinal LN, and MLN assessed by flow cytometry 15 h after i.v. injection. The values indicate frequency of $CFSE^{hi}$ cells (right peak) relative to $CFSE^{lo}$ cells (left peak) remaining from single mice, representative of two independent experiments with three to four mice per group in each experiment.

killing in vivo is regarded as essential for a successful HIV vaccine (17). Therefore, mice primed with rAdHu5 HIV-1 CN54 gag by dried MA or by i.d. injection were challenged i.v. on day 14 with carboxyfluorescein succinimidyl ester (CFSE)-labeled syngeneic targets pulsed with HIV-1 CN54 $gag_{309–318}$ peptide and control targets and cytotoxicity were analyzed after 15 h by flow cytometry. Comparable and robust in vivo killing was observed in spleen, inguinal, and MLN of mice immunized by the MA or i.d. route (Fig. 3*C*). Hence, a dried rAdHu5 HIV-1 gag MA vaccine generated robust $CD8^+$ effector T-cell responses of similar immunogenicity to the cognate vaccine in liquid suspension by i.d. injection.

Rapid Dermal Penetration, Dissolution and Dissemination Characterize Air-Dried MA Delivery. We next sought to determine the early events after MA application to the skin, because such information is germane to understanding their mechanism of delivery and safety. To track entry and dissolution in skin, MAs were fabricated to include FITC or TR-dextran in the matrix. Immunofluorescence microscopy of frozen mouse skin sections (dissected 30 min after application to the dorsal surface) confirmed disruption of the epidermis and FITC-dextran lining the perforation site (Fig. S4). Deeper in the dermis, at sites distant from the entry point, a FITC-dextran deposition also was shown, seemingly reflecting diffusion locally within 30 min (Fig. S4). Intravital confocal microscopy and Langerin-EGFP reporter mice were used to visualize the dynamics of MA penetration and TR-dextran (MA content) release in relation to DCs mobilization in back skin. Circular punctures within the LC network of the epidermis (20 μm below the surface) created by MA entry were observed 5 min after application (Fig. 4*A*, *Top* and *Middle*). At the same time within the dermis (at depths of 100 μm or greater), circular flaps of epidermis (distinguished by Langerin EGFP expression) were observed that superimposed with TR-dextran of the needle shaft, consistent with propulsion of the epidermis into the dermis at the entry site (Fig. 4*A*, *Top* and *Bottom*). Perforation of the epidermis was rapidly reduced, ostensibly reflecting skin retraction within 20 min, coincident with diffusion of the TR-dextran needle cargo into the surrounding epidermis (Fig. 4*B*). Intravital imaging at intervals

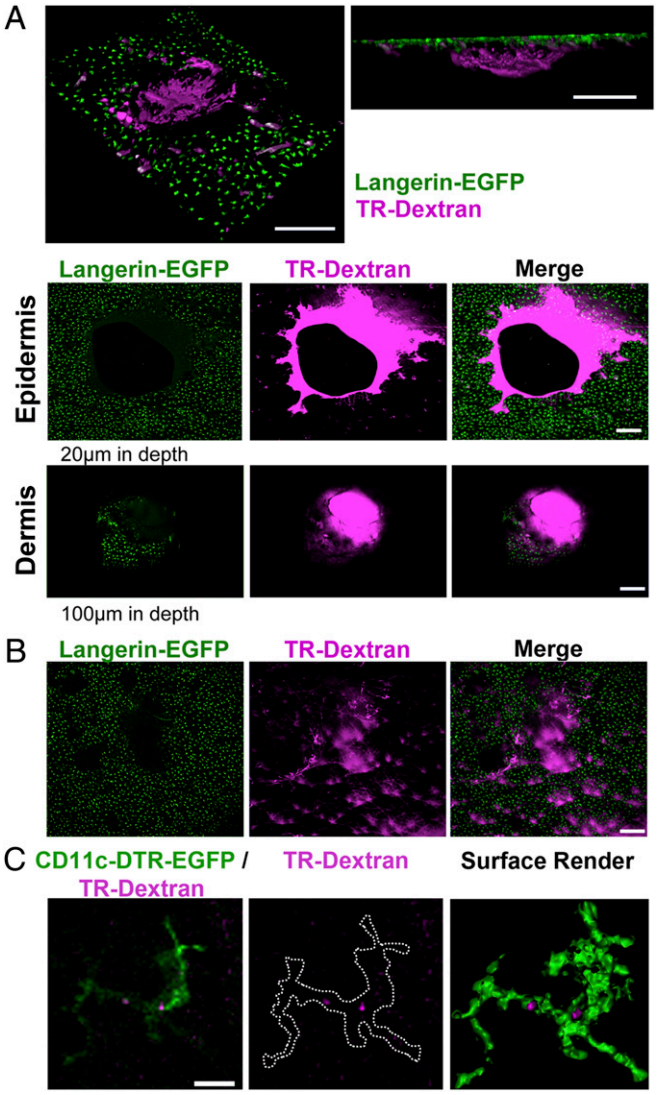

Fig. 4. Dried MAs penetrate the epidermis and dermis with rapid dissolution and dissemination of fluorescent cargo from the entry site. (*A*) *Top* shows representative Z-stack from approximate 100-μm-thick virtual section of the tissue, which is angled to show en-face (*Left*) or projected in Z (*Right*). Representative intravital confocal images (single Z-section) of epidermis (*Middle*) and dermis (*Bottom*) from Langerin-DTR-EGFP mice 5 min after TR-dextran MA application. Green, LCs; magenta, TR-dextran. Note perforation of epidermis with TR-dextran deposited around needle entry site (*Top*) and circular flap of epidermis containing LCs (green) in dermis coincident with TR-dextran needle shaft. (*B*) Intravital confocal images show TR-dextran (magenta) dissolved within LC network of Langerin-DTR-EGFP epidermis 20 min after TR-dextran MA application. (A and B) Similar observations were made in at least three additional experiments. (*C*) Colocalization of TR-dextran delivered by MA and CD11c-EGFP cells in dermis of CD11c-DTR-EGFP mice. Images show the following: single optical sections (3 μm thick) of $CD11c^+$ cells (green) and TR-dextran (magenta) (*Left*); TR-dextran alone with outline of CD11c expressing cell (*Center*); and surface rendered z-stacks with "clipping layers" applied to GFP fluorescence (green) to reveal areas of TR-dextran (magenta) in CD11c-DTR-EGFP skin, 1–3 h after TR-dextran MA application (*Right*). (Scale bars: *A* and *B*, 200 μm; *C*, 10 μm.)

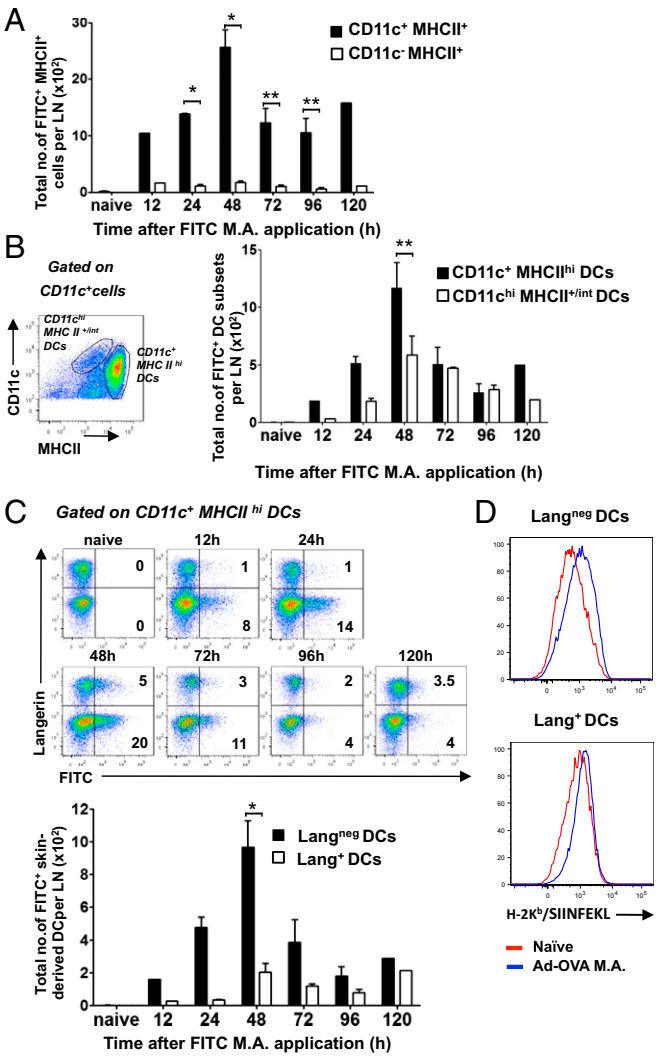

Fig. 5. Lang^{neg} DCs are the major population presenting MHC I-restricted Ag after skin application of rAdHu5 MAs. MAs containing AdHu5-OVA and FITC-dextran (*A*–*C*) or AdHu5-OVA only (*D*) were applied to dorsal foot skin. At indicated times; low density enriched popliteal LN cells were analyzed by FACS. Total mean numbers of FITC$^+$ APCs (gated on MHCII$^+$ cells) (*A*) and total mean numbers of FITC$^+$ skin-derived DCs (gated on CD11c$^+$ MHCII^{hi} cells) and LN resident DCs (gated on CD11c^{hi}MHCII$^{+/int}$ cells) (*B*). Bars represent the total mean number ± SEM from three independent experiments $*P < 0.05$, $**P < 0.001$ by one-way ANOVA with Tukey–Kramer post hoc test. (*C*) Dot plots (*Upper*) representative of three independent experiments show FITC$^+$ skin-derived DCs (from CD11c$^+$ MHCII^{hi} gate) expressing Langerin in draining LN cells. Percentages indicate FITC$^+$ Lang$^+$ and FITC$^+$ Lang^{neg} DCs in quadrants. Bars (*Lower*) indicate total mean number ± SEM of each subset from three independent experiments $*P < 0.05$. (*D*) K^b/SIINFEKL expression revealed by directly conjugated 25-D1.16 mAb by draining LN DC subsets 40 h after AdHu5-OVA MA application. Data are representative of two independent experiments of K^b/SIINFEKL expression on CD11c$^+$ MHCII^{hi} gated Lang$^+$ (*Lower*) and Lang^{neg} (*Upper*) DCs in draining LN of naïve and AdHu5-OVA MA immunized mice.

within 24 h did not reveal any colocalization of GFP-bearing LCs and TR-dextran in the vicinity of a needle entry point or in more distal zones, or detectable movement of LCs within the epidermis. In contrast, after application of MAs containing TR-dextran to CD11c-diphtheria toxin receptor (DTR)-EGFP reporter mice, CD11c-expressing cells within the dermis were observed to contain small amounts of TR-dextran (Fig. 4*C*, Fig. S5, and Movie S1), indicating acquisition of the MA.

Lang^{neg} DCs Are a Major Population Presenting MHC I-Restricted Ag After MA Immunization. To probe which DCs contribute to the CD8$^+$ T-cell response primed by live rAdHu5 virus-vectored MA vaccination, we first examined how rAdHu5 MAs applied to the dorsal skin of the foot influenced the relative number and kinetics of skin migrant and LN-resident DCs accumulating in popliteal LNs. FITC-dextran incorporated in the rAdHu5 MA was used as a surrogate for Ag uptake and DC labeling in the setting of virus-induced DC mobilization. Skin-draining low-density enriched LN cells revealed a peak of FITC$^+$CD11c$^+$MHCII$^+$ APCs at 48 h after MA application and a second (but reduced) peak at 120 h (Fig. 5*A*). This increase in FITC$^+$ cells was principally accounted for by skin-derived CD11c$^+$MHCII^{hi} DCs ($P < 0.001$) (18) compared with blood migratory/LN resident CD11c^{hi}MHCII$^{+/int}$ DCs (18) (Fig. 5*B*). Strikingly, the FITC$^+$ cells were predominantly Lang^{neg} as opposed to Lang$^+$CD11c$^+$MHCII^{hi} DCs ($P < 0.05$) at 48 h, consistent with migratory (presumably dermal) DCs mobilized by rAdHu5 MA application (Fig. 5*C*). Similar data were seen in FITC$^-$ DC subsets consistent with preferential accumulation of Lang^{neg} as opposed to Lang$^+$CD11c$^+$MHCII^{hi} DCs. Of note, within the quantitatively smaller FITC$^+$Lang$^+$ DC population, more than 90% were CD8α$^-$CD103$^-$ LCs with infrequent CD8α$^-$CD103$^+$ dermal DCs (Figs. S6 and S7). Together, these data indicate that although the MA cargo is distributed through the epidermis and dermis (Fig. 4), Lang^{neg} DCs presumably of dermal origin, as opposed to LCs or Lang$^+$ dermal DCs, predominantly accumulate in draining LNs after exposure to a cargo of rAdHu5 (Fig. 5*C*). Consistent with this finding, Lang^{neg}CD11c$^+$MHCII^{hi} DCs isolated from skin draining LNs 40 h after immunization with rAdHu5-OVA MAs demonstrated a marked increase in surface K^b/SIINFEKL complexes detected by directly conjugated 25-D1.16 mAb (19) compared with naïve mice (Fig. 5*D*) and stimulated proliferation of cocultured naïve CD8$^+$ OT-1 T cells in vitro (Fig. S8). Some presentation by Lang^{neg} LN-resident DCs (in addition to the Lang^{neg} migratory DCs) cannot be completely excluded in these assays based on gating strategy (Fig. S8) because activated LN-resident DC upregulate MHCII. It is noteworthy that Lang$^+$CD11c$^+$MHCII^{hi} DCs revealed little change in surface K^b/SIINFEKL expression (Fig. 5*D*). Taken together, these data are consistent with the conclusion that Lang^{neg}CD11c$^+$MHCII^{hi} DCs are a major population presenting MHC I-restricted Ag after MA immunization.

CD8$^+$ T-Cell Responses Induced by rAdHu5-OVA MAs Depend on CD11c$^+$ DCs but Are Largely Independent of LCs and CD8$^+$Lang$^+$ DCs. To explore the functional in vivo APC requirements for priming naïve CD8$^+$ T cells in the context of rAdHu5-OVA MA immunization, we used C57BL/6 (B6)-CD11c-EGFP-DTR mice that express a GFP-diphtheria toxin receptor (DTR) fusion protein under the control of the CD11c promoter (20), allowing for conditional ablation of dermal CD11c$^+$ cells after DT injection, but retention of LCs, which, although expressing CD11c, cannot be depleted in this model (ref. 21, Fig. 6). As expected, the frequency of SIINFEKL-specific CD8$^+$ T cells in spleen after MA immunization was significantly reduced in DT-treated mice when cross-compared with untreated mice ($P < 0.05$; Fig. 6). Conversely, ablation of Lang$^+$ cells by DT treatment of B6-Langerin-EGFP-DTR mice, as revealed by depletion of LCs in the epidermis and dermal Lang$^+$ DC (Fig. 7) and Lang$^+$ DC in draining LN, had a small but not significant impact on CD8$^+$ T-cell priming ($P = 0.2789$; Fig. 7). Therefore, LCs or Lang$^+$ DCs are not required to initiate CD8$^+$ T-cell priming by dissolvable live rAdHu5 virus-vectored MAs.

Discussion

Live recombinant Ad and poxvirus vectors hold promise as vaccines against HIV, malaria, and TB (1–3, 22). However, major technical challenges remain in terms of their delivery and stability for their realization to counter global disease burden. Hence, there is intense interest in technological advances to achieve live vector thermostability coupled with a delivery platform exploiting DC

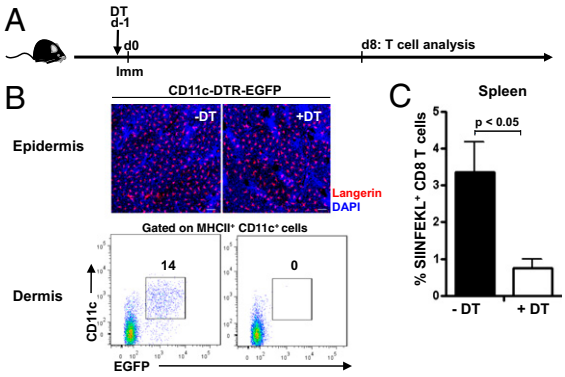

Fig. 6. Dependence of CD11c$^+$ dermal DCs for CD8$^+$ T-cell priming by rAdHu5-OVA MAs. (*A*) Schematic of K^b/SIINFEKL$^+$ CD8$^+$ T-cell assessment in CD11c-DTR-EGFP mice treated with or without DT 24 h before immunization with rAdHu5-OVA MA. (*B*) Confocal images show freshly isolated epidermal sheets from untreated CD11c-DTR-EGFP mice (-DT) and 3 d after DT treatment (+DT). Langerin (detected by anti-Langerin Ab, red), DAPI (blue). Dot plots show dermal cell suspensions within the CD45$^+$ MHC II$^+$ gate from skin of CD11c-DTR-EGFP mice: untreated (*Left*) and 3 d after DT treatment (*Right*). Data are representative of four mice per condition from two independent experiments. (*C*) Frequency of K^b/SIINFEKL$^+$ CD8$^+$ T cells in spleen 8 d after immunization of (-DT) untreated and (+DT) treated mice. Data are mean ± SEM of four mice per group; experiment repeated on two independent occasions with comparable results. $P < 0.05$.

biology to induce potent cellular immunity. Here, we reveal several important technical advances and mechanistic insights. We demonstrate the fabrication of a dissolvable MA containing a live recombinant AdHu5 vector that maintains thermostability and bioactivity, enables facile skin delivery, and evokes multifunctional, cytolytic CD8$^+$ T-cell responses in mice equipotent to that evoked by conventional needle delivery with live virus vector. Importantly, we have deciphered the contributions of the major DC subtypes in CD8$^+$ T-cell priming by this vaccine platform. Unexpectedly, Lang$^+$ CD103$^+$ DC subsets were not required for CD8$^+$ T-cell priming. In fact, we show migratory Lang^{neg} CD103^{neg} DCs more efficiently presented MHC class I-restricted rAdHu5 vector-derived Ag. Also, CD11c$^+$ MHCII^{hi} CD8α^{neg} EpCAM^{neg} CD11b$^+$ DCs (which are the migratory Lang^{neg} CD103^{neg} DCs) were fully capable of stimulating naïve CD8$^+$ T cells in vitro. These data suggest migratory/skin-derived Lang^{neg} DC subsets are sufficient for CD8$^+$ T-cell priming in the absence of Lang$^+$ DCs, likely by a direct route of Ag presentation but conceivably also indirectly as cross-dressed Ag, a mechanism of Ag presentation by CD8α$^-$ DCs for which there is increasing evidence (23, 24).

Whereas previous studies cited the capacity of model protein Ags and inactivated or subunit vaccine Ags to prime adaptive immunity via microfabrication technology (6–10), our study has advanced this platform for live Ad vectors. This modality brought additional challenges: maintaining conformation of the rAdHu5 capsid proteins sufficient to enable virus host receptor binding, internalization, and nuclear targeting coupled with integrity of the adenoviral genome to enable transcriptional competence for Ag expression. Slow drying rAdHu5 vectors in a sucrose formulation to a dry state demonstrated no loss in transgene immunogenicity for at least 1 mo after reconstitution, in agreement with a previous report (25). Crucially, to enable greater practical applicability in the field, we advanced this approach by incorporation of a stabilized rAdHu5 HIV-1 gag vaccine vector within the matrix of a dissolvable MA, thus removing the necessity for vaccine reconstitution and hypodermic needle delivery. Effector CD8$^+$ T-cell responses induced by MA immunization were comparable both in magnitude and functionality (cytokine production and cytolysis) to those achieved by conventional needle injection, including i.d. Moreover, robust CD8$^+$ T-cell responses were also found in gut mucosal tissues and their associated lymphoid tissues. We have not yet defined whether this finding is a function of DCs mobilized by the MA delivery system, or a function of the vector, because it is reported that innate DC programming by rAdHu5 promotes intestinal CD8$^+$ T-cell recruitment (15, 26), although likely both mechanisms operate. Nonetheless, the capacity to elicit mucosal CD8$^+$ T cells highlights the potential of the live MA vaccine vector delivery platform to confer protection against mucosal pathogens.

T-cell priming by microfabricated vaccine delivery platforms is attributed to Ag capture and/or presentation by LCs (6, 8–10). Indeed, our confocal imaging revealed fluorescent MA cargo distributed within the epidermis and dermis, hence potentially accessible to epidermal resident LCs, and LCs either trafficking through the dermis (27) or propelled to the dermis at the site of needle entry. Nevertheless, after rAdHu5-vectored MA immunization, we found no evidence for significant accumulation of Lang$^+$ CD8α$^-$CD103$^-$ LCs in skin draining LNs, or presentation of Ag (K^b/SIINFEKL complexes) by skin-derived Lang$^+$ DCs, which include canonical LCs. Equally, Lang$^+$ DCs (including LCs) were functionally dispensable for CD8$^+$ T-cell priming in the setting of DT-treated Langerin-DTR mice, consistent with a redundancy in LCs priming CD8$^+$ T cells in skin infection (13, 28, 29).

In the absence of LCs, at least two additional dermal CD11c$^+$ MHCII^{hi} DC subsets—the Lang$^+$ CD103$^+$ DCs and a heterogeneous Lang^{neg}CD103$^-$ DC subset (12)—could contribute to CD8$^+$ T-cell priming by an rAdHu5 MA vector delivery platform. Although, Lang$^+$CD103$^+$ DCs demonstrate an impressive ability for cross-presentation (12, 29) numerically, these DCs are significantly less abundant than Lang^{neg}CD103$^-$ DCs (12). Moreover, in contrast to the Lang^{neg} CD11c$^+$ MHCII^{hi} migratory DCs, the Lang$^+$CD103$^+$ DC subset showed little change in surface K^b/SIINFEKL complexes. Thus, it appears that after rAdHu5 MA vector immunization, Lang^{neg} DCs more efficiently present MHC class I-restricted rAdHu5 vector-derived Ag. Indeed, the Lang^{neg} DCs are the only skin-derived subset that remains in DT-treated Langerin-DTR mice. Conceivably, Lang^{neg} DCs express an enhanced capacity for rAdHu5 infection and/or transcriptional competence and, thereby, present Ag directly to CD8$^+$ T cells. At the same time, it is noteworthy that a subset of skin-derived Lang^{neg} DCs with the capacity for

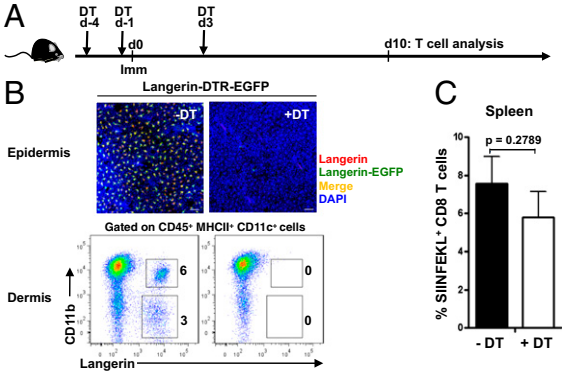

Fig. 7. Lang$^+$ DCs are dispensable for CD8$^+$ T-cell priming by rAdHu5-OVA MAs. (*A*) Schematic of DT treatment (day −4, −1, and +3) relative to rAdHu5-OVA MA immunization in Langerin-DTR-EGFP mice and K^b/SIINFEKL$^+$ CD8$^+$ T-cell assessment on day 10. (*B*) Confocal images show freshly isolated epidermal sheets from untreated Langerin-DTR-EGFP mice (-DT) and 3 d after final DT treatment (+DT): red, Langerin (detected by anti-Langerin Ab); green, Langerin-EGFP; yellow-orange, merge; blue, DAPI. Dot plots show dermal DCs defined by CD11b and Langerin within the CD45$^+$ MHC II$^+$ gate from skin cells of Langerin-DTR-EGFP mice: untreated (*Left*) and 3 d after final DT treatment (*Right*). Data are representative of four mice per condition from three independent experiments. (*C*) Frequency of K^b/SIINFEKL$^+$ CD8$^+$ T cells in spleen 10 d after immunization of (-DT) untreated and (+DT) treated mice. Data are mean ± SEM of four mice per group; experiment repeated on three independent occasions with comparable results. $P = 0.2789$ by Student's *t* test.

in vivo cross-presentation of *Candida albicans*-derived Ag has been reported (13). Equally, given recent evidence for acquisition of cross-dressed Ag from parenchymal cells (24) and as intact MHC:peptide complexes donated from other DCs (23), the possibility exists that Lang^{neg} DCs contained within the CD8α$^-$ population have the capacity to present cross-dressed Ag to CD8$^+$ T cells.

In conclusion, we have shown that a live recombinant AdHu5 vector fabricated as a thermostable, dissolvable MA induces potent multifunctional, cytolytic CD8$^+$ T-cell responses in mice, highlighting an important technical advance to enable the possibility of live vector stability and delivery in a global context. These data may have important implications for recombinant viral vaccine vectors advancing to the clinic and shed light on the early events after MA delivery, indicating a striking redundancy in the role of LCs or Lang$^+$ DCs in priming naïve CD8$^+$ T-cell responses and also the possibility that multiple routes of Ag presentation operate after MA vaccination.

Materials and Methods

Full details of methods are described in *SI Materials and Methods*.

Recombinant E1, E3-Deleted Adenovirus Vaccines. AdHu5-OVA virus encoding a nonsecreted OVA was a gift from M. Zenke (Aachen University, Aachen, Germany). AdHu5 HIV-1 gag [encoding a codon optimized synthetic HIV-1 CN54-gag gene; Geneart] (Fig. S9) is described in *SI Materials and Methods*. Viruses were propagated by The Native Antigen Company Ltd.

Fabrication of Microneedle Arrays. Arrays were fabricated by a centrifugation casting method using a 1 cm^2 inverted cone-shaped silicone template comprising 44 needles, each 1,500 μm in height and 670 μm in base diameter as detailed in *SI Materials and Methods*. For DC tracking experiments, MAs contained both rAdHu5-OVA and TR or FITC-labeled dextran.

Immunization of Mice. MAs were applied to the dorsal surface of the foot, the ear, or the back skin of mice. Additional groups of mice received the equivalent rAdHu5-vector dose, by the i.m., i.d., or s.c. route. All in vivo procedures were performed in accordance with United Kingdom Home Office regulations and Kings College London ethics committee.

Conditional Depletion of CD11c$^+$ and Langerin$^+$ Cells. Depletions were performed by using *CD11c-DTR-EGFP* and *Lang-DTR-EGFP* mice treated with DT.

Intravital Confocal Microscopy. TR-dextran MAs were applied to the shaved skin of *Lang-EGFP or CD11c-EGFP-DTR* mice and imaged.

Reagents for Flow Cytometry. SIINFEKL peptide was purchased from GenScript and HIV-1 gag$_{309–318}$ peptide and PE-labeled K^b/SIINFEKL pentamer from ProImmune. Allophycocyanin-labeled D^b/GVKNWMTDTL tetramer was provided by the University of Washington, Seattle.

Analysis of Polyfunctional CD8$^+$ T-Cell Responses. Spleen cells were restimulated with anti-CD28 either alone or with OVA$_{257–264}$ or HIV-1 CN54 gag$_{309–318}$ peptides and stained for IFN-γ, IL-2, and TNF-α or CD107.

In Vivo Killing Assay. Splenocytes were labeled with CFSE at 5 μM (CFSE^{hi}) or 0.5 μM (CFSE^{lo}), pulsed with or without HIV-1 CN54 gag$_{309–318}$ peptide, then injected into immunized mice and harvested after 15 h.

Statistical Analysis. Bars in figures show the mean ± SEM. A two-tailed Student *t* test was performed when comparing two different conditions. A one-way ANOVA with a Tukey–Kramer post hoc test were used to analyze three or more conditions. *P* value <0.05 was considered significant.

ACKNOWLEDGMENTS. We thank Dr. M. Allen (King's College London) for help with cryostat sectioning and Prof. Adrian Hayday for critically reviewing the manuscript. This work is supported in part by the Bill and Melinda Gates Foundation Collaboration for AIDS Vaccine Discovery and a European Union Sixth Framework Programme Network of Excellence (European Vaccines and Microbicides Enterprise) award.

1. Barouch DH, et al. (2012) Vaccine protection against acquisition of neutralization-resistant SIV challenges in rhesus monkeys. *Nature* 482(7383):89–93.
2. García F, et al. (2011) Safety and immunogenicity of a modified pox vector-based HIV/AIDS vaccine candidate expressing Env, Gag, Pol and Nef proteins of HIV-1 subtype B (MVA-B) in healthy HIV-1-uninfected volunteers: A phase I clinical trial (RISVAC02). *Vaccine* 29(46):8309–8316.
3. Hansen SG, et al. (2011) Profound early control of highly pathogenic SIV by an effector memory T-cell vaccine. *Nature* 473(7348):523–527.
4. Brandau DT, Jones LS, Wiethoff CM, Rexroad J, Middaugh CR (2003) Thermal stability of vaccines. *J Pharm Sci* 92(2):218–231.
5. Melnick JL (1996) Thermostability of poliovirus and measles vaccines. *Dev Biol Stand* 87:155–160.
6. Sullivan SP, et al. (2010) Dissolving polymer microneedle patches for influenza vaccination. *Nat Med* 16(8):915–920.
7. Widera G, et al. (2006) Effect of delivery parameters on immunization to ovalbumin following intracutaneous administration by a coated microneedle array patch system. *Vaccine* 24(10):1653–1664.
8. Zhu Q, et al. (2009) Immunization by vaccine-coated microneedle arrays protects against lethal influenza virus challenge. *Proc Natl Acad Sci USA* 106(19):7968–7973.
9. del Pilar Martin M, et al. (2012) Local response to microneedle-based influenza immunization in the skin. *MBio* 3(2):e00012–e12.
10. Fernando GJ, et al. (2010) Potent immunity to low doses of influenza vaccine by probabilistic guided micro-targeted skin delivery in a mouse model. *PLoS ONE* 5(4): e10266.
11. Prausnitz MR, Mikszta JA, Cormier M, Andrianov AK (2009) Microneedle-based vaccines. *Curr Top Microbiol Immunol* 333:369–393.
12. Henri S, et al. (2010) CD207+ CD103+ dermal dendritic cells cross-present keratinocyte-derived antigens irrespective of the presence of Langerhans cells. *J Exp Med* 207(1):189–206.
13. Igyártó BZ, et al. (2011) Skin-resident murine dendritic cell subsets promote distinct and opposing antigen-specific T helper cell responses. *Immunity* 35(2):260–272.
14. Lee JW, Park JH, Prausnitz MR (2008) Dissolving microneedles for transdermal drug delivery. *Biomaterials* 29(13):2113–2124.
15. Kaufman DR, et al. (2008) Trafficking of antigen-specific CD8+ T lymphocytes to mucosal surfaces following intramuscular vaccination. *J Immunol* 181(6):4188–4198.
16. Lindsay RW, et al. (2010) CD8+ T cell responses following replication-defective adenovirus serotype 5 immunization are dependent on CD11c+ dendritic cells but show redundancy in their requirement of TLR and nucleotide-binding oligomerization domain-like receptor signaling. *J Immunol* 185(3):1513–1521.
17. McMichael AJ, Borrow P, Tomaras GD, Goonetilleke N, Haynes BF (2010) The immune response during acute HIV-1 infection: Clues for vaccine development. *Nat Rev Immunol* 10(1):11–23.
18. Lee HK, et al. (2009) Differential roles of migratory and resident DCs in T cell priming after mucosal or skin HSV-1 infection. *J Exp Med* 206(2):359–370.
19. Porgador A, Yewdell JW, Deng Y, Bennink JR, Germain RN (1997) Localization, quantitation, and in situ detection of specific peptide-MHC class I complexes using a monoclonal antibody. *Immunity* 6(6):715–726.
20. Jung S, et al. (2002) In vivo depletion of CD11c+ dendritic cells abrogates priming of CD8+ T cells by exogenous cell-associated antigens. *Immunity* 17(2):211–220.
21. Bennett CL, Clausen BE (2007) DC ablation in mice: Promises, pitfalls, and challenges. *Trends Immunol* 28(12):525–531.
22. Hoft DF, et al. (2012) A recombinant adenovirus expressing immunodominant TB antigens can significantly enhance BCG-induced human immunity. *Vaccine* 30(12): 2098–2108.
23. Smyth LA, et al. (2012) Acquisition of MHC:peptide complexes by dendritic cells contributes to the generation of antiviral CD8+ T cell immunity in vivo. *J Immunol* 189(5):2274–2282.
24. Wakim LM, Bevan MJ (2011) Cross-dressed dendritic cells drive memory CD8+ T-cell activation after viral infection. *Nature* 471(7340):629–632.
25. Alcock R, et al. (2010) Long-term thermostabilization of live poxviral and adenoviral vaccine vectors at supraphysiological temperatures in carbohydrate glass. *Sci Transl Med* 2(19):19ra12.
26. Ganguly S, Manicassamy S, Blackwell J, Pulendran B, Amara RR (2011) Adenovirus type 5 induces vitamin A-metabolizing enzymes in dendritic cells and enhances priming of gut-homing CD8 T cells. *Mucosal Immunol* 4(5):528–538.
27. Kissenpfennig A, et al. (2005) Dynamics and function of Langerhans cells in vivo: Dermal dendritic cells colonize lymph node areas distinct from slower migrating Langerhans cells. *Immunity* 22(5):643–654.
28. Allan RS, et al. (2003) Epidermal viral immunity induced by CD8alpha+ dendritic cells but not by Langerhans cells. *Science* 301(5641):1925–1928.
29. Bedoui S, et al. (2009) Cross-presentation of viral and self antigens by skin-derived CD103+ dendritic cells. *Nat Immunol* 10(5):488–495.